The Cryosphere Discuss., 6, 715–735, 2012
www.the-cryosphere-discuss.net/6/715/2012/
doi:10.5194/tcd-6-715-2012

The Cryosphere Discussions

Longer spring snowmelt: spatial and temporal variations of snowmelt trends detected by passive microwave from 1988 to 2010 in the Yukon River Basin

K. A. Semmens and J. M. Ramage

Lehigh University, Bethlehem, Pennsylvania, USA

Received: 2 February 2012 – Accepted: 5 February 2012 – Published: 17 February 2012

Correspondence to: K. A. Semmens (kas409@lehigh.edu)

Published by Copernicus Publications on behalf of the European Geosciences Union.

Abstract

Brightness temperature (T_b) data from the Special Sensor Microwave Imager (SSM/I) 37 V-GHz frequency provides a time series from 1988 to 2010 that enables the assessment of snowmelt timing trends (onset, end of melt-refreeze, and duration) for the Yukon River Basin. T_b and diurnal amplitude variation (DAV) thresholds determine dates of melt onset and melt-freeze end (end of high DAV), defined as the first date when thresholds are met for more than three of five consecutive days. Temporal and spatial trends in melt onset and end of melt-refreeze date are determined with varying time period intervals and for each sub-basin and elevation class. Earlier melt onset trends are found in the highest elevations and northernmost sub-basins (Porcupine, Chandalar, and Koyukuk Rivers). Significant later ($>0.75\,\mathrm{d\,yr^{-1}}$) end of melt-refreeze and longer melt duration trends are found in a majority of the sub-basins. Moving interval trends suggest interannual variability within the time series and a power spectrum analysis reveals peak frequencies and periods of 5–7 and ~11 years, possibly related to El Nino- Southern Oscillation and the solar cycle, respectively. Latitude and elevation display the dominant controls on timing variance and spring solar flux is highly correlated with melt timing in middle elevations.

1 Introduction

Arctic air temperature has increased at twice the global rate for the past several decades with more recent warming appearing strongest in winter and spring, critical seasons for snow accumulation and melt and first leaf/bloom (McBean et al., 2005; Schwartz et al., 2006). Projections for the middle of the 21st century include: increases in average air temperatures of 3 °C for the Arctic by 2040, increases in precipitation in mid to high latitudes leading to overall deeper arctic snow cover, and increases in snowmelt and runoff for cold regions (Adam et al., 2009). The snowpack integrates effects of changes over several months, resulting in the strongest shifts to the

TCD
6, 715–735, 2012

hydrological cycle predicted for the early spring melt period; especially since snowmelt dominated basins are the most sensitive to temperature increases in the winter (Nijssen et al., 2001). It is hypothesized that such shifts will be reflected in the timing of snowmelt onset in the spring and the end of the melt-refreeze period, a transitional period where the snowpack is melting during the day and refreezing at night. The timing of this high diurnal variation period of melt-refreeze affects the progression of meltwater through a basin, corresponding to the snow off date (which is usually a few days to weeks later dependent on maximum snow accumulation), freshet timing, and peak snowmelt runoff, and is closely linked to green-up and growing season start (Cayan et al., 2001; Schwartz et al., 2006; Wang et al., 2011). Further, for high latitude drainage basins, snowmelt, peak runoff, and associated flooding are the most important and significant hydrologic event each year (Kane, 1997; Rouse et al., 1997; Yang et al., 2009). Melt timing has a critical influence on the annual hydrological cycle: with early melt, the snowmelt period may be longer, snow gradually depleted, and runoff spread out, but with late melt, the snowmelt is rapid, synchronous, and peak runoff high (Woo and Thorne, 2006). Thus changes in snowmelt timing and streamflow seasonality impact the availability of water resources in snowmelt-dominated basins, affecting populations that rely on seasonal snowpacks for their water supply (Barnett et al., 2005). Snowmelt timing and related runoff may also affect and be affected by wildfire occurrence whose frequency, intensity, and associated landscape changes are altered by the changing climate (Westerling et al., 2006; Shakesby and Doerr, 2006).

Assessment of snowmelt timing trends provides evidence for changes in snowmelt timing and associated runoff which may be indicative of hydrologic shifts (Serreze et al., 2000; Yang et al., 2002, 2009). Snowmelt trends for the pan-Arctic as detected by microwave brightness temperatures (T_b) from the Scanning Multichannel Microwave Radiometer (SMMR) and the Special Sensor Microwave Imager (SSM/I) have been previously assessed for 1979–2008 (Tedesco et al., 2009). The melt onset and melt end dates were found to have significant negative trends with melt starting 0.5 d yr^{-1} earlier and ending 1 d yr^{-1} earlier over the past 30 years, thus showing a shortened

TCD
6, 715–735, 2012

melt season of 0.6 d yr^{-1} (Tedesco et al., 2009). Melt onset and snow-off dates for the pan-arctic were also detected from enhanced resolution SeaWinds scatterometer QuikSCAT data from 2000-2005 using a melt algorithm that identifies multiple melt events, their duration and intensity, comparing differences between daily time series radar data and the previous five day average (Wang et al., 2008). Results from the QSCAT melt detection revealed that melt onset occurred in the middle to the end of March for boreal forest areas, increased with latitude, and was later over high elevation areas and for years with a cold spring season. Melt end dates were later over lake-rich areas and had more interannual variability than onset dates, while melt duration was longer for areas with deeper snow cover (Wang et al., 2008). An integrated pan-Arctic melt onset date dataset from active and passive microwave satellites further elucidated melt progression over various land types and determined that elevation, tree fraction and latitude largely explained mean melt onset date in the terrestrial Arctic (Wang et al., 2011).

Here we investigate spatial and temporal trends in date of snowmelt onset and end of melt-refreeze detected utilizing passive microwave T_b data from the Special Sensor Microwave Imager (SSM/I). The analysis focuses on the Yukon River Basin (YRB) for the (combined) years of record 1988 to 2010. The YRB is one of the largest basins in North America, stretching from northwestern Canada to the Bering Sea through Alaska and drains 853 300 km^2 crossing from northwestern Canada through central Alaska, covering several ecoregions, and discharging an annual mean discharge of 6400 m^3 s^{-1} of water and 60 million tons of sediment at its mouth to the Bering Sea annually (Brabets et al., 2000). Most of the 13 sub-basins of the Yukon can be characterized by a subarctic nival regime with snowmelt driving runoff, but some have significant glacier runoff, particularly the White and Tanana River basins (Brabets et al., 2000; Woo et al., 2008). The large range of elevations, permafrost type, and runoff regime among sub-basin provides a basis for analyzing factors influencing trends in snowmelt timing. Given the rising temperature trends and projections for this area, the basin is vulnerable to permafrost degradation, making it ideal for studying its sensitivity to warming temperatures

TCD
6, 715–735, 2012

(Walvoord and Striegl, 2007). For the YRB, modeling studies suggest earlier snowmelt timing of longer duration, diminished snow cover, and increased runoff and erosion due to permafrost thawing (Walvoord and Striegl, 2007; Hay and McCabe, 2010). A water balance model forced with IPCC climate simulations to project potential hydrological responses to climate change in the YRB for the 21st century indicate increased runoff (largest for May to July), later snow accumulation start, and earlier snowmelt start with the largest temperature changes in the winter (Hay and McCabe, 2010).

This study, focusing on one river basin, as opposed to previous pan-arctic studies, provides a more detailed investigation of trends and governing factors, especially focusing on elevation differences. It is hypothesized the most significant differences will occur between basins based on their range of elevations; as such, the analysis will focus on elevation classes of 200 m intervals (based on average elevation of each pixel) within each sub-basin. Elevation was found to relate to snowmelt for the Sierra Nevada where 1500 to 2100 m elevations contributed 10–15 % of snowmelt, 2100 to 3000 m elevations 40–60 %, and areas above 3000 m 30–40 % with each higher band of elevation melting out 2 to 3 weeks later than the band below (Rice et al., 2011).

2 Data and methods

Snowmelt detection. Melting snow is detectable by passive microwave sensors because the presence of liquid water within a snowpack increases its emissivity, thus increasing T_b which is a function of the surface temperature (T_s) and emissivity (ε) of the material ($T_b = \varepsilon T_s$). Therefore there is a significant difference in T_b between wet (emits close to that of a blackbody) and dry snow (Chang et al., 1975; Ulaby et al., 1986). Wet snow grains result in an increase in loss tangent (quantification of dissipation of electromagnetic energy of a dielectric material) and thus a scattering albedo of near zero and emissivity near unity which explains the rapid increase in T_b for melting snow (Chang et al., 1976). Higher frequency wavelengths are sensitive to the shallow depths of snowpack while lower frequencies can penetrate deeper. Here the 37 GHz

TCD
6, 715–735, 2012

vertically polarized wavelength is used due to its high sensitivity to water in the snowpack (Ramage et al., 2006). Previous studies have shown snow cover distribution and snowmelt timing are adequately measured by passive microwave sensors daily, in all weather conditions (Hall et al., 1991; Mote et al., 1993; Drobot and Anderson, 2001; Ramage and Isacks, 2002; Wang et al., 2005; Ramage et al., 2006; Apgar et al., 2007; Tedesco, 2007; Tedesco et al., 2009).

SSM/I data, provided by the National Snow and Ice Data Center (NSIDC), are in the form of Level 3 Equal-Area Scalable Earth (EASE)-Grid Brightness Temperatures gridded data for Northern Hemisphere projection, have a resolution of $37 \times 28\,km^2$ gridded to EASE-Grid $25 \times 25\,km^2$ with two observations per day at overpass times around 8:30 and 18:30 PST (Armstrong et al., 1994). For a continuous data record from 1988 to 2010, SSM/I data from DMSP F8, F11, F13, and F17 satellites are combined. Specifically, years 1988–1991 are from F8, 1992–1995 are F11, 1996–2007 are F13, and 2007–2010 are F17. While others have used linear regression equations to correct data between the different satellites, in general the biases due to a switch in satellites are minimal and not statistically significant, with regression coefficients affecting data by generally less than 0.5 percent (Abdalati et al, 1995; Stroeve et al., 1998; Cavalieri et al., 1999; Meier et al., 2001). There is high consistency among the SSM/Is' brightness temperatures suggesting differences are minimal (Dai and Che, 2009). Additionally, intercalibration is best when there is a long overlap between satellites, preferably at least a year so that seasonal differences can be accounted for, thus adjustments based on short overlapping time periods may be less accurate and introduce bias (Stroeve et al., 1998). Based on these findings and on a manual overview of the data, no correction was deemed necessary given the risk of introduction of new unknown bias.

SSM/I data and the technique for detecting snowmelt timing has been previously established in the upper YRB using 37 GHz vertically polarized data (Ramage et al., 2006) and has been found to correlate well with higher resolution Advanced Microwave Scanning Radiometer – EOS (AMSR-E) derived snowmelt onset (Apgar et al., 2007). The twice-daily observations enable the calculation of the running difference between

TCD
6, 715–735, 2012

the ascending and descending brightness temperature values termed the diurnal amplitude variation or DAV, which is a proxy of the dynamism of the snowpack as liquid water content changes (Ramage and Isacks, 2002). High DAV values, especially for 37 GHz sensitive to the top centimeter of snowpack, indicate when the snowpack is melting during the day and re-freezing at night (Ramage et al., 2006). Snowmelt onset is determined from SSM/I data (37 GHz vertically polarized) when T_b is greater than 246 K and DAV are above ±10 K, thresholds previously developed and validated (Ramage and Isacks, 2002; Ramage et al., 2006). Melt onset (and end high DAV/melt-refreeze) are defined as the first date when at least three of five consecutive days meet the T_b and DAV thresholds described above. Melt transition duration is the length in days from melt onset to end of melt-refreeze. The three of five day algorithm has proven accurate based on manual cross checking of observations and correspondence with estimates from earlier work, and allows the melt onset and melt-refreeze end to be automatically detected for large regions such as the YRB. A similar approach was previously utilized with QSCAT where melt onset was identified when the difference was greater than a threshold for three or more consecutive days and the intensity calculated as the accumulated decrease in radar cross section in relation to the five day mean (Wang et al., 2008).

It is important to note that there are some limitations and sources of error for this approach including the coarse resolution of the SSM/I data which does not account for sub-grid variability. We assume that the same thresholds apply across all sub-basins, areas, and SSM/I sensors (Ramage et al., 2006). If a pixel has a significant sub-portion melting (but not all) it will be detected as wet. Additionally, these methods assume the terrain is relatively homogeneous and the snowmelt signal is not distorted by land cover and topography, thus there is some uncertainty due to vegetation, mixed pixels, sub-grid variability, and high relief (Mätzler et al., 1998). With regard to snow water equivalent, Foster et al. (2005) found errors to be highest with deep snow, dense forests, and fast growing crystals with topography having less of an effect on the passive microwave retrievals than vegetation. Dong et al. (2005) found errors associated

TCD
6, 715–735, 2012

with snow pack mass and distance to open water, among other sources. While these studies focus on SWE, they are illustrative of the sources of error and uncertainty working with passive microwaves (e.g. Foster et al. 2005, and references therein). In the present study, pixels close to the coast in the Lower Yukon sub-basin were excluded from the analysis to reduce errors associated with coastal regions.

Trend Analysis. Trends in the date of melt onset and end of melt-refreeze were calculated from linear regression with trend significance determined using the p value from the two-tailed student's t-test after testing for normal distribution and auto-correlation. These trends were determined from average dates of melt timing based on sub-basin as well as elevation class with elevation binned by 200 m intervals (0–200; 3001–3200, etc.). Pixels were grouped into elevation class based on the average elevation determined from a 30 arc sec digital elevation map (Long and Brabets, 2002). SSM/I derived melt timing trends were calculated for (1) the whole period 1988–2010, (2) a 7 year moving average within the whole period, (3) an increasing trend length starting at 1988 with trend end years ranging from 1998 to 2010, and (4) the period 2003–2010 in order to compare to the AMSR-E dataset. The variable trend end year approach was successfully utilized in previous studies of sea ice extent (Kay et al., 2011) and for investigating individual streamflow patterns in watersheds (Zhang et al., 2010). While the Mann-Kendall (M-K) test has been predominately used in previous studies of streamflow trends (Burn and Hag Elnur, 2002; Burn et al., 2010), here regression and t-test analyses were conducted in lieu of the M-K test in order to be able to characterize the pattern of the trend, its rapidity and when and how the trend changes. Further, based on trend analysis of annual streamflow in Turkey, the parametric t-test and M-K test can be used interchangeably, with the t-test being more powerful for normally distributed datasets (Önöz and Bayazi, 2003).

Signal processing of the dataset was conducted with a discrete Fourier transformation from which the power spectrum was analyzed to determine peak frequency and period for each basin and each elevation class. Solar flux at 10.7 cm wavelength (National Research Council of Canada, 2011) was analyzed against the average melt

TCD
6, 715–735, 2012

onset and melt-refreeze date for each elevation class. Further, anomalies from the 1981–2010 climatology for air temperature at 850 mb and sea level pressure from the NCEP/NCAR reanalysis (Kalnay et al., 1996) were used as proxies for atmospheric circulation patterns to compare to temporal trends for correlative and multiple regression analysis.

3 Results

Various time interval approaches were investigated to assess the trends in melt onset, end of melt-refreeze, and melt transition duration from the 23 year SSM/I record. First, to distinguish spatial patterns of trends, the whole time period is shown for each sub-basin among the range of elevations in 200 m intervals (Fig. 1a, d, g). A distinct pattern of earlier melt onset (Fig. 1a) occurs in the highest elevations and in the northernmost sub-basins generally underlain with continuous permafrost, however, the trends are not significant. The majority of elevations and basins show no significant change in onset with the exception of slightly later onset in the Lower Yukon, but this may reflect the more maritime climate or the prevalence of wetlands which can affect the T_b signature. In contrast to melt onset, end of melt-refreeze trends (Fig. 1d) are toward later timing, are significant, and have high R^2 values. The later trends tend to be in the middle elevations and latitudes such as in the Upper, Stewart, Pelly, White, Teslin, and Yukon headwater sub-basins. Longer melt duration trends are significant and occur throughout the YRB with the exception of no change in the lowest elevations (Fig. 1g).

To better understand the temporal variability of the detected trends, time intervals were systematically increased with variable end years, starting with a ten year period from 1988 to 1998 and extending to a 23 year period from 1988 to 2010 (Fig. 1b, e, h). Earlier trends (not significant but large R^2) occur for melt onset but as the time interval increases in length these are muted to essentially no change in onset (Fig. 1b), suggesting alternating sub-trends. In contrast, end of melt-refreeze (and melt duration) shows a later (and longer) trend for the majority of the basins through most of the time

TCD
6, 715–735, 2012

intervals investigated which are, in general, statistically significant (Fig. 1e, h). These trends persist regardless of the length of interval, indicative of robustness.

To get a sense of the sub-trends affecting the longer term trends, a 7 year moving interval window was used for analysis where each column is the trend for the 7 year time period starting with each year from 1988 to 2003 (Fig. 1c, f, i). There is a distinct pattern from earlier melt onset (>0.75 d yr^{-1} earlier) in the beginning of the 23 year period to later onset in the middle of the period and back to earlier onset at the end of the period for the majority of the basins (Fig. 1c). The two main exceptions are the lower elevation West Central and Lower Yukon sub-basins which have a later onset trend in the later years. The earlier onset trends are not statistically significant whereas the later onset trends are, though both tend to have high R^2 values. The trend for end of melt-refreeze is earlier (but not significant) in the beginning of the time series which transitions to a later (and highly significant, high R^2) trend, then a non-significant (but high R^2) earlier trend for years 1998-2001, and finally a significant later trend in the last two periods (Fig. 1f). Stemming from the onset and end trends, the melt duration trends exhibit a lengthening, then a shortening (non-significant but high R^2), and back to lengthening towards the end of the time series (Fig. 1i). These alternations suggest a sub-trend cyclic pattern such as ENSO.

Due to the cyclic pattern reflected in the 7 year moving average time interval analyses, the dataset was processed to extract power spectrum, peak frequency, and period for each sub-basin (Table 1). The solar cycle (~11 years) is apparent in several of the basins' melt onset (Chandalar, Tanana, Upper Yukon, Stewart, and Yukon Headwaters) while shorter 5–7 year periods possibly related to ENSO are also apparent in some basins (Porcupine, Pelly, White, and Teslin), as well as short ~3 year periods. End of melt-refreeze appears more related to ENSO type 5–7 year cycles as no basin showed the ~11 year solar cycle period.

Further elucidation of the cyclic nature of the melt onset and end of melt-refreeze signal was determined by subsetting by elevation class (Fig. 2). Melt onset is dominated by shorter periods in the lower elevation basins, while the longer ~11 year sun cycle

TCD
6, 715–735, 2012

is reflected in the higher elevations in the Tanana and in the northern basins Koyukuk and Chandalar Rivers. The areas that had earlier melt onset trends are those whose signal has a peak with a period of 11.5 years. The end of melt-refreeze signal is much less variable with the majority of the YRB reflecting the ~7 year cycle (possibly related to ENSO). Exceptions are the higher elevations of the Tanana and Stewart which show the 11.5 year period and the low-lying Upper Yukon and Porcupine which show shorter 3–4 year periods.

Multiple regression with average elevation, latitude, longitude, and composite (October to April for each year) anomalies from NCEP/NCAR Reanalysis (Kalnay et al., 1996) for sea level pressure and air temperature at 850 mb explain 47.4 % of the variance for end of melt-refreeze timing, 60.7 % of variance for melt onset timing, and 38 % of the variance for melt duration. In particular, for end of melt-refreeze, average elevation was most strongly correlated (0.44), followed by longitude (0.21). For melt onset, latitude was most strongly correlated (0.32) followed by average elevation (0.29). For melt duration, the strongest correlation was with latitude (–0.34) followed by elevation (0.21). All correlations were significant with p-values < 0.0001. These results support the initial hypothesis that elevation exhibits a dominant control on melt timing (albeit more strongly for melt-refreeze than melt onset) within the sub-basins. Figure 3 is further illustration of the strong correlation between solar flux and melt timing. Latitude and elevation were previously found to be important factors influencing mean melt onset date (Wang et al., 2011).

4 Discussion and conclusions

Trend analysis of snowmelt onset, end of melt-refreeze, and melt duration in the sub-basins of the YRB from 1988 to 2010 reveals significant lengthening of melt transition duration throughout much of the basin with earlier melt onset in high elevations and the northernmost basins (Porcupine, Chandalar, and Koyukuk Rivers) and significant later end of melt-refreeze in the intermediate elevations and latitudes. Melt onset is most

TCD
6, 715–735, 2012

strongly correlated with spring solar flux especially in high elevations and northern sub-basins. The visibility of the effect of solar cycles at middle and high latitudes seen in periodicities with the ∼11 year basic solar frequency was also found by Tomasino and Valle (2000) in their analysis of multiple historical hydrometeorological datasets.

Varying the time intervals for trend analysis enabled elucidation of inter-annual variability and sub-trends possibly related to circulation patterns. Power spectrum analysis reveals peak frequencies and periods of 5–7 and ∼11 years, possibly related to ENSO and the solar cycle, respectively. Differences are most notable among differing elevations with lower elevations illustrating shorter cycles and higher elevations tending to reflect longer cycles. These shorter frequency cycles may serve to mute the overall trend of the basins due to the relatively short time series analyzed (23 years). The prevalence of snow in high elevations have a buffering effect on changes while lower elevation snow variability may suggest climate change susceptibility (Rice et al., 2011), both factors that can influence the timing trends presented here.

The melt timing trend variability for the YRB reflect multiple influencing factors, however, solar flux and elevation are dominant controls and the overall pattern is toward longer melt duration for the spring snowmelt transition period which has significant implications for snowmelt runoff and associated flooding, as well as green-up and first leaf dates. Additionally, the trend analysis highlights the importance of choice of time period for analysis and the need to investigate varying time intervals in order to understand the dynamics of trends.

Acknowledgements. SSM/I data provided by National Snow and Ice Data Center. NCEP Reanalysis data provided by the NOAA/OAR/ESRL PSD, Boulder Colorado, USA. Semmens is supported by NASA Headquarters under the NASA Earth and Space Science Fellowship – Grant "NNX10AP14H".

TCD
6, 715–735, 2012

References

Abdalati, W., Steffen, K., Otto, C., and Jezek, K. C.: Comparison of brightness temperatures from SSMI instruments on the DMSP F8 and F11 satellites for Antarctica and the Greenland ice sheet, Int. J. Remote Sens., 16, 1223–1229, 1995.

Adam, J. C., Hamlet, A. F., and Lettenmaier, D. P.: Implications of global climate change for snowmelt hydrology in the twenty-first century, Hydrol. Proc., 23, 962–972, 2009.

Apgar, J. D., Ramage, J. M., McKenney, R. A., and Maltais, P.: Preliminary AMSR-E Algorithm for Snowmelt Onset Detection in Subarctic Heterogeneous Terrain, Hydrol. Proc., 21, 1587–1596, 2007.

Armstrong, R. L., Knowles, K. W., Brodzik, M. J., and Hardman, M. A.: DMSP SSM/I Pathfinder Daily EASE-Grid Brightness Temperatures [1988–2010], Boulder, Colorado USA: National Snow and Ice Data Center, 1994.

Barnett, T. P., Adam, J. C., and Lettenmaier, D. P.: Potential impacts of a warming climate on water availability in snow-dominated regions, Nature, 438, 303–309, 2005.

Brabets, T. P., Wang, B., and Meade, R. H.: Environmental and hydrologic overview of the Yukon River Basin, Alaska and Canada, USGS Water-Resources Investigations Report 99-4204, Anchorage, Alaska, 2000.

Burn, D. H. and Hag Elnur, M. A.: Detection of hydrologic trends and variability, J. Hydrol., 255, 107–122, 2002.

Burn, D. H., Sharif, M., and Zhang, K.: Detection of trends in hydrological extremes for Canadian watersheds, Hydrol. Proc., 24, 1781–1790, 2010.

Cavalieri, D. J., Parkinson, C. L., Gloersen, P., Comiso, J. C., and Zwally, J. H.: Deriving long-term time series of sea ice cover from satellite passive-microwave multisensory data sets, J. Geophys. Res., 104, 15803–15814, 1999.

Cayan, D. R., Kammerdiener, S. A., Dettinger, M. D., Caprio, J. M., and Peterson, D. H.: Changes in the onset of spring in the western United States, Bull. Am. Meterol. Soc., 82, 399–415, 2001.

Chang, A. T. C. and Gloersen, P.: Microwave emission from dry & wet snow, Operational Applications of Satellite Snow Cover Observations: 399–407, NASA, SP 391, Washington, DC, 1975.

Chang, A. T. C., Gloersen, P., Schmugge, T., Wilheit, T. T., and Zwally, H. J.: Microwave emission from snow and glacier ice, J. Glaciol., 16, 23–39, 1976.

TCD
6, 715–735, 2012

Dai, L. and Che, T.: Cross-platform calibration of SMMR, SSM/I and AMSR-E passive microwave brightness temperature, Sixth International Symposium on Digital Earth: Data Processing and Applications, Proc. of SPIE 7841, 784103, 2009.
Dong, J., Walker, J. P., and Houser, P. R.: Factors affecting remotely sensed snow water equivalent uncertainty, Remote Sens. Environ., 97, 68–82, 2005.
Drobot, S. and Anderson, M.: An improved method for determining melting onset dates over Arctic sea ice using scanning multichannel microwave radiometer and Special Sensor Microwave/Imager data, J. Geophys. Res., 106, 24033–24049, 2001.
Foster, J. L., Sun, C., Walker, J. P., Kelly, R., Chang, A., Dong, J., and Powell, H.: Quantifying the uncertainty in passive microwave snow water equivalent observations, Remote Sens. Environ., 94, 187–203, 2005.
Hall, D. K., Sturm, M., Benson, C. S., Chang, A. T. C., Foster, J. L., Garbeil, H., and Chacho, E.: Passive microwave remote and in situ measurements of arctic and subarctic snow covers in Alaska, Remote Sens. Environ., 38, 161–172, 1991.
Hay, L. E. and McCabe, G. J.: Hydrologic effects of climate change in the Yukon River Basin, Climatic Change, 100, 509–23, 2010.
Kalnay, E., Kanamitsu, M., Kistler, R., Collins, W., Deaven, D., Gandin, L., Iredell, M., Saha, S., White, G., Woollen, J., Zhu, Y., Leetmaa, A., Reynolds, R., Chelliah, M., Ebisuzaki, W., Higgins, W., Janowiak, J., Mo, K.C., Ropelewski, C., Wang, J., Jenne, R., and Joseph, D.: NCEP/NCAR 40-yr reanalysis project, Bull. Am. Meteor. Soc., 77, 437–470, 1996.
Kane, D. L.: The impact of Arctic hydrologic perturbations on Arctic ecosystems induced by climate change, Global Change and Arctic Terrestrial Ecosystems, Ecological Studies 124, Spring-Verlag: New York, 63–81, 1997.
Kay, J. E., Holland, M. M., and Jahn, A.: Inter-annual to multi-decadal Arctic sea ice extent trends in a warming world, Geophys. Res. Lett., 38, L15708, 2011.
Long, D. and Brabets, T. P.: Coverage YUK_DEM National Stream Quality Accounting Network (NASQAN) Yukon River Basin, Canada and Alaska Basin, Yukon River, 2002.
Mätzler, C., Hiltbrunner, D., and Standley, A.: Relief effects for passive microwave remote sensing, WP330, SNOW-TOOLS, Research Report No. 98-3, 1998.
McBean, G., Alekseev, G., Chen, D., Førland, E., Fyfe, J., Groisman, P. Y., King, R., Melling, H., Vose, R., and Whitfield, P. H.: Arctic climate: past and present, Arctic Climate Impacts Assessment (ACIA), Cambridge University Press, Cambridge, 21–60, 2005.
Meier, W. N., Khalsa, S. J. S., and Savoie, M. H.: Intersensor calibration between F-13 SSM/I

TCD
6, 715–735, 2012

and F-17 SSMIs near-real-time sea ice estimates, IEEE T. Geosci. Remote Sens., 49, 3343–3349, doi:10.1109/TGRS.2011.2117433, 2011.

Mote, T. L., Anderson, M. R., Kuivinen, K. C., and Rowe, C. M.: Passive microwave-derived spatial & temporal variations of summer melt on Greenland ice sheet, Ann. Glaciol., 17, 233–238, 1993.

National Research Council of Canada: 10.7 cm Solar Flux Data, ftp://ftp.ngdc.noaa.gov/STP/SOLAR{_}DATA/SOLAR{_}RADIO/FLUX/Penticton{_}Observed/monthly/MONTHLY.OBS, 2011.

Nijssen, B., O'Donnell, G. M., Hamlet, A. F., and Lettenmaier, D. P.: Hydrologic sensitivity of global rivers to climate change, Climatic Change, 30, 143–175, 2001.

Önöz, B. and Bayazi, M.: The power of statistical tests for trend detection, Turkish J. Eng. Env. Sci., 27, 247–251, 2003.

Ramage, J.M. and Isacks, B.L.: Determination of melt-onset and refreeze timing on southeast Alaskan icefields using SSM/I diurnal amplitude variations, Annals of Glaciology, 34, 391-398, 2002.

Ramage, J. M., McKenney, R. A., Thorson, B., Maltais, P., and Kopczynski, S. E.: Relationship between passive microwave-derived snowmelt and surface-measured discharge, Wheaton River, Yukon, Hydrol. Proc., 20, 689–704, 2006.

Rice, R., Bales, R. C., Painter, T. H., and Dozier, J.: Snow water equivalent along elevation gradients in the Merced & Tuolumne River basins, Sierra Nevada, Water Resour. Res., 47, W08515, 2011.

Rouse, W. R., Douglas, M. S. V., Hecky, R. E., Hershey, A. E., Kling, G. W., Lesack, L., Marsh, P., McDonald, M., Nicholson, B. J., Roulet, N. T., and Smol, J. P.: Effects of climate change on the freshwaters of Arctic and Subarctic North America, Hydrol. Proc., 11, 873–902, 1997.

Schwartz, M. D., Ahas, R., and Aasa, A.: Onset of spring starting earlier across the North Hemisphere, Global Change Biol., 12, 343–351, 2006.

Serreze, M. C., Walsh, J. E., Chapin III, F. S., Osterkamp, T., Dyurgerov, M., Romanovsky, V., Oechel, W. C., Morison, J., Zhang, T., and Barry, R. G.: Observational evidence of recent change in the northern high-latitude environment, Climatic Change, 46, 159–207, 2000.

Shakesby, R. A. and Doerr, S. H.: Wildfire as a hydrological and geomorphological agent, Earth-Sci. Rev., 74, 269–307, 2006.

Stroeve, J., Maslanik, J., and Xiaoming, L.: An intercomparison of DMSP F11- and F13-derived sea ice products, Remote Sens. Environ., 64, 132–152, 1998.

TCD
6, 715–735, 2012

Tedesco, M.: Snowmelt detection over the Greenland ice sheet from SSM/I brightness temperature daily variations, Geophys. Res. Lett., 34, L02504, 2007.
Tedesco, M., Brodzik, M., Armstrong, R., Savoie, M., and Ramage, J.: Pan arctic terrestrial snowmelt trends from spaceborne passive microwave data and correlation with the AO, Geophys. Res. Lett., 36, L21402, 2009.
Tomasino, M. and Valle, F. D.: Natural climatic changes and solar cycles: an analysis of hydrological time series, Hydrol. Sci. J., 45, 477–489, 2000.
Ulaby, F. T., Moore, R. K., and Fung, A. K.: Microwave Remote Sensing: Active and Passive, Vol. III: From Theory to Applications, Artech House: Dedham, 1986.
Walvoord, M. A. and Striegl, R. G.: Increased groundwater to stream discharge from permafrost thawing in the Yukon River basin: Potential impacts on lateral export of carbon and nitrogen, Geophys. Res. Lett., 34, L12402, 2007.
Wang, L., Sharp, M., Brown, R., Derksen, C., and Rivard, B.: Evaluation of spring snow covered area depletion in Canadian Arctic, NOAA snow charts, Remote Sens. Environ., 95, 453–63, 2005.
Wang, L., Derksen, C., and Brown, R.: Detection of pan-arctic terrestrial snowmelt from QuikSCAT, 2000–2005, Remote Sens. Environ., 112, 3795–3805, 2008.
Wang, L., Wolken, G. J., Sharp, M. J., Howell, S. E. L., Derksen, C., Brown, R. D., Markus, T., and Cole, J.: Integrated pan-Arctic melt onset detection from satellite active and passive microwave measurements, 2000–2009, J. Geophys. Res., 116, D22103, 2011.
Westerling, A. L., Hidalgo, H. G., Cayan, D. R., and Swetnam, T. W.: Warming and earlier spring increase western US forest wildfire activity, Science, 313, 940–943, 2006.
Woo, M. K. and Thorne, R.: Snowmelt contribution to discharge from large mountainous catchment in subarctic Canada, Hydrol. Proc., 20, 2129–2139, 2006.
Woo, M. K., Thorne, R., Szeto, K., and Yang, D.: Streamflow hydrology in boreal region under the influences of climate and human interference, Phil. Trans. R. Soc. B, 363, 2251–2260, 2008.
Yang, D., Kane, D. L., Hinzman, L. D., Zhang, X., Zhang, T., and Ye, H.: Siberian Lena River hydrologic regime and recent change, J. Geophys. Res., 107, 4694, 2002.
Yang, D., Zhao, Y., Armstrong, R., and Robinson, D.: Yukon River streamflow response to seasonal snow cover changes, Hydrol. Proc., 23, 109–121, 2009.
Zhang, Z., Dehoff, A. D., and Pody, R. D.: New approach to identify trend pattern of streamflows, J. Hydrol. Eng., 15, 244–248, 2010.

TCD
6, 715–735, 2012

Table 1. Peak periodicity for each Yukon River sub-basin. Period, peak, and peak frequency from signal processing and power spectrum analysis using discrete Fourier transformation of the melt onset dates (onset) and end of melt-refreeze dates (end) for the 13 sub-basins. Units for period and peak are years.

Sub-basin	Onset Period	Onset Peak	Onset Freq.	End Period	End Peak	End Freq.
Porcupine	5.75	7.32	0.17	7.67	9.79	0.13
Chandalar	11.5	14.4	0.09	7.67	12.0	0.13
Koyukuk	3.29	12.1	0.30	7.67	15.4	0.13
East Central	3.29	11.7	0.30	7.67	14.2	0.13
West Central	3.29	9.15	0.30	7.67	20.8	0.13
Tanana	11.5	7.04	0.09	7.67	12.9	0.13
Upper Yukon	11.5	9.34	0.09	7.67	15.0	0.13
Stewart	11.5	10.4	0.09	5.75	12.5	0.17
Pelly	5.75	14.9	0.17	5.75	18.1	0.17
White	5.75	7.84	0.17	3.29	19.3	0.30
Lower	4.60	18.1	0.22	7.67	33.8	0.13
Yukon Hdwtrs	11.5	8.08	0.09	3.29	25.2	0.30
Teslin	5.75	13.8	0.17	5.75	14.0	0.17

TCD
6, 715–735, 2012

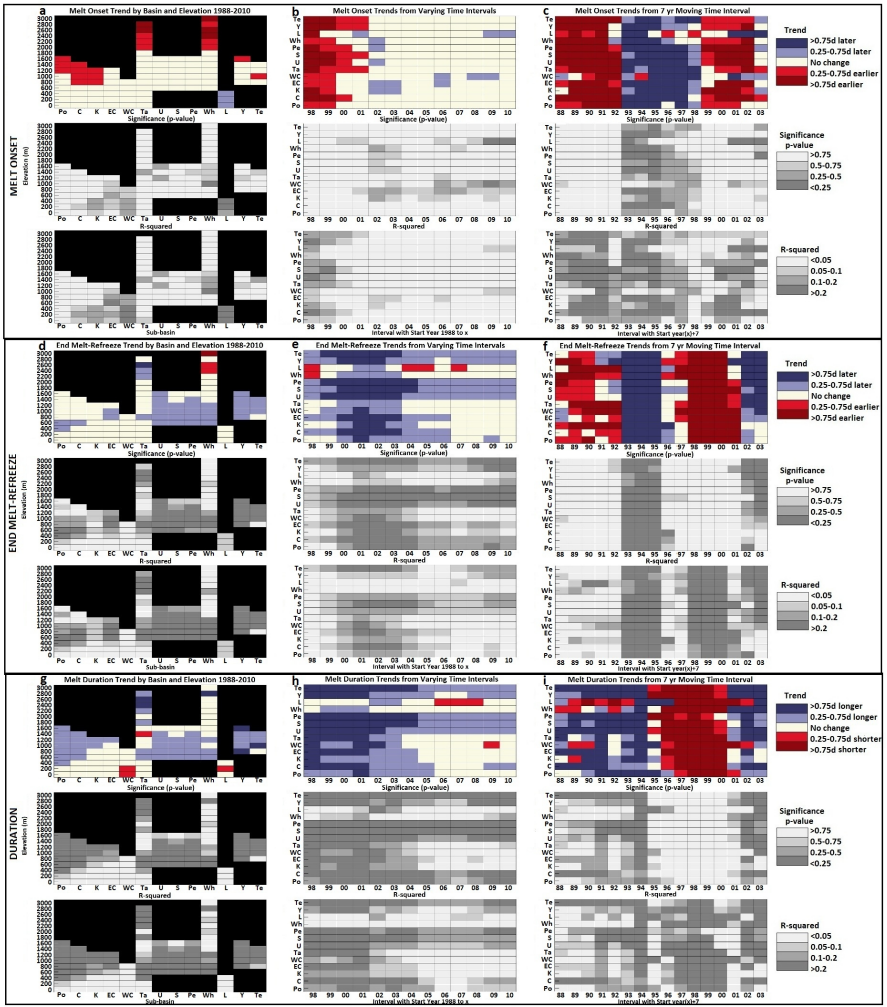

Fig. 1. Caption on next page.

TCD
6, 715–735, 2012

Longer spring snowmelt

K. A. Semmens and J. M. Ramage

Fig. 1. Spatial and Temporal Trends. In each panel **(a–i)** top plots are the direction and magnitude of trend (red is earlier melt and blue is later melt timing). Middle plots are the significance of the trends - p-value of student's t-test (darker is more significant). Bottom plots are the R^2 values (darker is higher R^2). Details described in a, b, and c also apply to all subsequent plots below. Trends, significance, and R^2 for (a) melt onset for each basin (columns) and elevation class (rows). The elevation label on the y-axis is the floor and the ceiling is 200 m higher. Black indicates no data for that basin and elevation. Basins are arranged from highest to lowest latitude (left to right). **(b)** Melt onset for each basin (rows) for varying time intervals (columns) – column 1 is the ten year period from 1988 to 1998 and each subsequent column is a year longer than the preceding. **(c)** Melt onset for each basin (rows) for a 7 year moving period (columns) with starting years 1988 to 2003. **(d)** End melt-refreeze elevation and basin. **(e)** End melt-refreeze variable time interval. **(f)** End melt-refreeze 7 year moving period. **(g)** Melt duration elevation and basin. **(h)** Melt duration variable time interval. **(i)** Melt duration 7 year moving period. Labels for basins are as follows: Po = Porcupine, C = Chandalar, K = Koyukuk, EC = East Central, WC = West Central, Ta = Tanana, U = Upper, S = Stewart, Pe = Pelly, Wh = White, L = Lower, Y = Yukon Headwaters, Te = Teslin.

TCD
6, 715–735, 2012

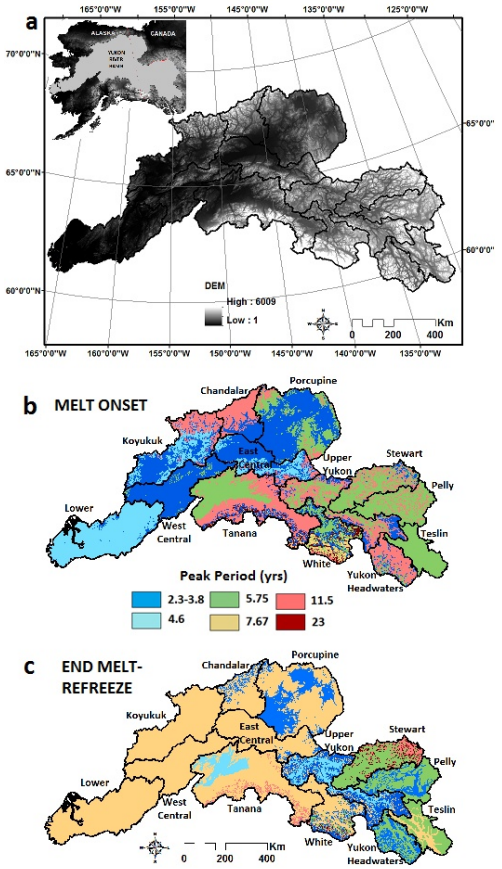

Fig. 2. Peak periods in melt timing trends. **(a)** Overview of study area and digital elevation map of the Yukon River Basin (Long and Brabets, 2002). Spatial distribution of peak periodicity for melt onset **(b)** and end of melt-refreeze **(c)**. Peak period key applies to both b and c.

TCD
6, 715–735, 2012

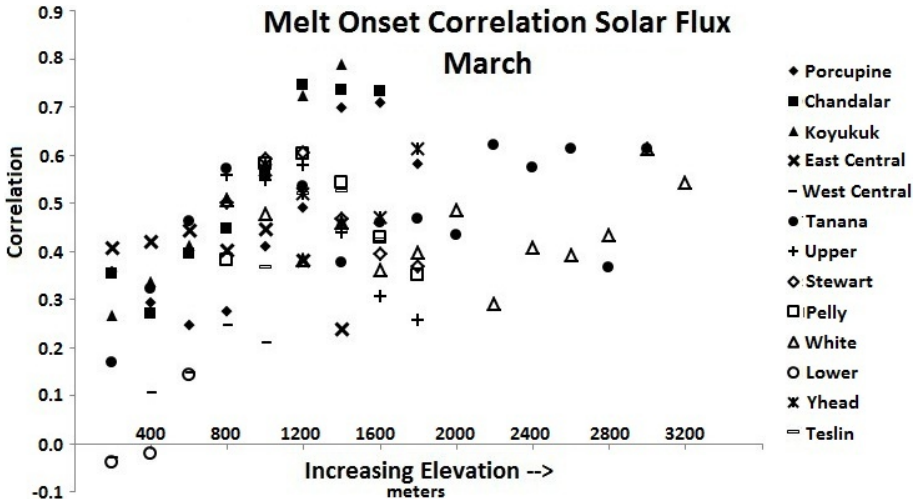

Fig. 3. Correlation of solar flux and melt onset date for each basin and elevation. Significant positive correlations are in high elevations and northern sub-basins which correspond to the peak ~11 year period shown in Fig. 2.

TCD
6, 715–735, 2012